

Detection of faint broad emission lines in type 2 AGN – II. On the measurement of the black hole mass of type 2 AGN and the unified model

F. Onori,^{1,2,3★} F. Ricci,³ F. La Franca,³ S. Bianchi,³ A. Bongiorno,⁴ M. Brusa,^{5,6}
F. Fiore,⁴ R. Maiolino,⁷ A. Marconi,^{8,9} E. Sani¹⁰ and C. Vignali^{5,6}

¹*SRON Netherlands Institute for Space Research, Sorbonnelaan 2, NL-3584 CA Utrecht, the Netherlands*

²*Department of Astrophysics/IMAPP, Radboud University, PO Box 9010, NL-6500 GL Nijmegen, the Netherlands*

³*Dipartimento di Matematica e Fisica, Università Roma Tre, via della Vasca Navale 84, I-00146 Roma, Italy*

⁴*INAF – Osservatorio Astronomico di Roma, via Frascati 33, I-00044 Monte Porzio Catone, Italy*

⁵*Dipartimento di Fisica e Astronomia, Università di Bologna, viale Bertoni 6/2, I-40127 Bologna, Italy*

⁶*INAF – Osservatorio Astronomico di Bologna, via Ranzani 1, I-40127 Bologna, Italy*

⁷*Cavendish Laboratory, University of Cambridge, 19 J. J. Thomson Avenue, Cambridge CB3 0HE, UK*

⁸*Dipartimento di Fisica e Astronomia, Università degli Studi di Firenze, Via G. Sansone 1, I-50019 Sesto Fiorentino, Italy*

⁹*INAF – Osservatorio Astronomico di Arcetri, Largo E. Fermi 5, I-50125 Firenze, Italy*

¹⁰*European Southern Observatory, Alonso de Cordova 3107, Casilla 19, Santiago 19001, Chile*

Accepted 2017 February 17. Received 2017 February 16; in original form 2016 October 29

ABSTRACT

We report the virial measurements of the black hole (BH) mass of a sample of 17 type 2 active galactic nuclei (AGN), drawn from the *Swift*/BAT 70-month 14–195 keV hard X-ray catalogue, where a faint BLR component has been measured via deep NIR (0.8–2.5 μm) spectroscopy. We compared the type 2 AGN with a control sample of 33 type 1 AGN. We find that the type 2 AGN BH masses span the $5 < \log(M_{\text{BH}}/M_{\odot}) < 7.5$ range, with an average $\log(M_{\text{BH}}/M_{\odot}) = 6.7$, which is ~ 0.8 dex smaller than found for type 1 AGN. If type 1 and type 2 AGN of the same X-ray luminosity $\log(L_{14-195}/\text{erg s}^{-1}) \sim 43.5$ are compared, type 2 AGN have 0.5 dex smaller BH masses than type 1 AGN. Although based on few tens of objects, this result disagrees with the standard AGN unification scenarios in which type 1 and type 2 AGN are the same objects observed along different viewing angles with respect to a toroidal absorbing material.

Key words: galaxies: active – quasars: emission lines – quasars: supermassive black holes – galaxies: Seyfert – infrared: galaxies.

1 INTRODUCTION

In the last decade, by using hard X-ray (2–10 keV) selected active galactic nuclei (AGN) samples, it has been possible to accurately derive the AGN luminosity function up to $z \sim 6$ (e.g. Ueda et al. 2014). Moreover, by using virial-based techniques in the optical band on samples of broad line type 1 AGN (AGN1), it has been possible to estimate the supermassive black hole (BH) mass function (e.g. Greene & Ho 2007; Kelly et al. 2010; Schulze et al. 2015). However, the BH mass (M_{BH}) measurements are affected by several selection biases against the narrow line type 2 AGN (AGN2), or low-luminosity AGN, where the broad-line region (BLR) is not visible in the rest-frame optical band because of either dust absorption or dilution by the host galaxy spectra (see e.g. Baldassare et al. 2016).

According to the original standard unified model (Antonucci 1993), the different observational classes of AGN

(AGN1 and AGN2) are believed to be the same kind of objects observed under different conditions (e.g. different orientations of the observer with respect to a dusty torus). In the framework of the AGN phenomenon and co-evolution, this implies that AGN with the same luminosity should share, on average, the same properties (e.g. same masses, same accretion rates and, then, same Eddington ratios $\lambda_{\text{Edd}} = L_{\text{bol}}/L_{\text{Edd}}$).

Nevertheless, nowadays there is growing evidence that AGN1 and AGN2 could belong to intrinsically different populations (see e.g. Elitzur 2012; Lanzuisi et al. 2015), having, on average, different luminosities (lower for AGN2; Ueda et al. 2003; La Franca et al. 2005; Ueda et al. 2014), different accretion rates (smaller for AGN2, Winter et al. 2010; Lusso et al. 2012), different host galaxy properties (more late-type for AGN2), and different clustering, environment and halo mass properties (Allevato et al. 2014).

The observed difference in the luminosity distributions of AGN1 and AGN2 could, however, still comply with an orientation-based unified model in which the torus opening angle (or the absorbing material covering factor) depends on luminosity. In this scenario, many of the observed differences between the AGN1 and the AGN2

* E-mail: f.onori@sron.nl

population can be attributed to selection effects. In contrast, if a difference is measured in the average M_{BH} (or host halo mass and clustering properties) of AGN1 and AGN2 *sharing the same intrinsic (corrected for absorption) luminosity*, then AGN1 and AGN2 should be intrinsically different objects and the unified model should be revised.

We have therefore started a project aimed at measuring the BH mass in AGN2 (La Franca et al. 2015, 2016; Onori et al. 2017; Ricci et al. 2017). In those few studies where AGN2 BH masses have been derived (e.g. Heckman et al. 2004, from The Sloan Digital Sky Survey), the authors used the M_{BH} –host scaling relations that have not yet been proven to hold for such a population (see Graham 2008; Kormendy, Bender & Cornell 2011). Several studies have shown that many AGN2 exhibit faint broad-line components if observed with high (≥ 20) S/N in the near-infrared (NIR; 0.8–2.5 μm), where the dust absorption is less severe than in the optical (Veilleux, Goodrich & Hill 1997; Riffel, Rodríguez-Ardila & Pastoriza 2006; Cai et al. 2010). Moreover, observation in the NIR of AGN1, whose M_{BH} were measured using reverberation mapping techniques (RM; Blandford & McKee 1982; Peterson 1993) have demonstrated that the virial method to measure M_{BH} can be efficiently used with the NIR Pa α $\lambda 1.875 \mu\text{m}$ and Pa β $\lambda 1.282 \mu\text{m}$ lines (Kim, Im & Kim 2010; Landt et al. 2011).

Following the above studies and, as it is observed for the optical continuum luminosity, the empirical relation between the X-ray luminosity and the dimension of the BLR ($R_{\text{BLR}} \propto \sqrt{L}$; Maiolino et al. 2007; Greene et al. 2010), Ricci et al. (2017) have calibrated new virial relations between the FWHM_{NIR} of the most relevant NIR emission lines (Pa α , Pa β , He I $\lambda 1.083 \mu\text{m}$) and the intrinsic hard X-ray luminosity, L_X , of the type $M_{\text{BH}} \propto \text{FWHM}_{\text{NIR}}^2 L_X^{0.5}$. These relations can be used to measure M_{BH} of either AGN2 or obscured and low-luminosity AGN1 (see also La Franca et al. 2015, 2016).

In this paper, we present the measurement for M_{BH} of a sample of AGN2 selected from the *Swift*/BAT 70-month catalogue (Baumgartner et al. 2013), where a faint BLR component in the NIR emission line was found (Onori et al. 2017). We compare the resulting M_{BH} distribution with that of a control sample of AGN1 selected from the *Swift*/BAT 70-month catalogue and whose M_{BH} have been measured via RM techniques. We adopt a $\Omega_{\text{m}} = 0.3$, $\Omega_{\Lambda} = 0.7$ and $H_0 = 70 \text{ km s}^{-1} \text{ Mpc}^{-1}$ cosmology. Unless otherwise stated, all the quoted uncertainties are at 68 per cent confidence level.

2 DATA AND SAMPLES

In order to measure the BH mass of the AGN2, we have carried out NIR spectroscopic observations of 41 obscured and intermediate-class AGN (type 2, 1.9 and 1.8; all named AGN2 in the following) at redshift $z \lesssim 0.1$, randomly selected from the *Swift*/BAT 70-month catalogue. Thanks to the very hard X-ray band (14–195 keV) that has been used to build the catalogue, the parent AGN sample is free of absorption selection effects up to $\log N_{\text{H}} \lesssim 24 \text{ cm}^{-2}$ (see e.g. fig. 11 in Burlon et al. 2011). The observations have been carried out in the framework of a systematic study of the AGN2 NIR spectral properties and have been executed using ISAAC/VLT, X-shooter/VLT and LUCI/LBT spectrometers, with a spectral resolution of 65, 20–78 and 220 km s^{-1} , respectively, and reaching an average S/N ratio of ~ 30 per resolution element. A BLR component showing $800 < \text{FWHM} < 3500 \text{ km s}^{-1}$, significantly larger than the narrow-line region component measured in the same spectra, has been identified in 13 out of 41 AGN2 (~ 30 per cent of the total sample). The data reduction, spectral analysis and line fitting parameters (full width at half-maximum, FWHM, and fluxes

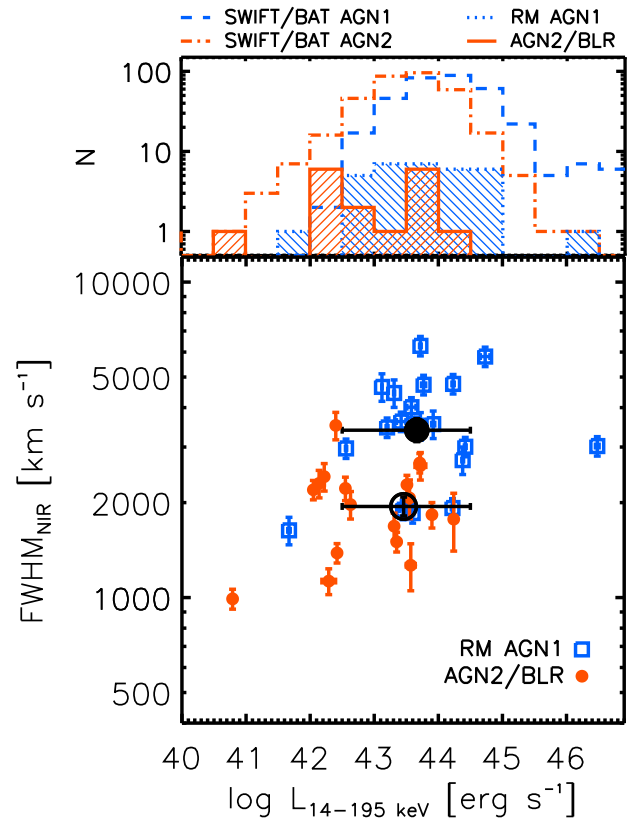


Figure 1. Top panel: distribution of L_{14-195} of the 17 AGN2/BLR, where a BLR component was found (red continuous line), and AGN1 control sample (blue dotted line). The red dot dashed and the blue dashed lines show the distribution of the complete AGN2 and AGN1 samples of the *Swift*/BAT 70-month catalogue, respectively. Bottom panel: average FWHM of the BLR of the NIR lines (Pa β and He I) of AGN1 (blue open squares) and AGN2/BLR (red filled circles) as a function of the intrinsic X-ray luminosity, L_{14-195} . The black filled (open) circle shows the FWHM average value of the total AGN1 (AGN2/BLR) sample in the $42.5 < \log(L_{14-195}/\text{erg s}^{-1}) < 44.5$ luminosity bin and has been plotted at the position of the average $\log L_{14-195}$.

of the most relevant emission lines) have been published in a companion paper (Onori et al. 2017). The sample has been extended with four AGN2 included in the *Swift*/BAT 70-month catalogue, whose FWHM NIR lines, or spectra, were available in the literature. The spectral data, when available, have been fitted using the technique described in Onori et al. (2017). In Table 1, we list the FWHM of the BLR components of the He I and Pa β lines of the AGN2 sample (in the following called AGN2/BLR sample).

In Fig. 1 (top panel), we show the L_{14-195} distributions of all the AGN2 included in the *Swift*/BAT 70-month catalogue (red dot-dashed line) as well as the distributions of the 17 AGN2/BLR (red continuous line). The average X-ray luminosity is $\log L_{14-195} = 43.5$ with a spread $\sigma(\log L_{14-195}) = 0.9$ and $\log L_{14-195} = 42.9 \text{ erg s}^{-1}$ with a spread $\sigma(\log L_{14-195}) = 0.9$, for the *Swift*/BAT AGN2 and the AGN2/BLR, respectively.

In order to build a control sample of AGN1 to be compared with the results obtained from the AGN2 population, we have used 33 AGN1 included in the *Swift*/BAT 70-month catalogue and whose M_{BH} have been measured via RM techniques. This sample includes those 31 AGN1 selected by Ricci et al. (2017, Table 1) plus two additional RM AGN1, namely 3C 390.3 ($\log L_{14-195} = 44.88 \text{ erg s}^{-1}$, $M_{\text{vir}} = 278_{-32}^{+24} \times 10^6 M_{\odot}$) and Mrk 50 ($\log L_{14-195} = 43.45 \text{ erg s}^{-1}$,

Table 1. The sample of AGN2/BLR and their BH masses.

Object name (1)	z (2)	Class (3)	A_V (mag) (4)	W2–W4 (mag) (5)	$\log(L_{14-195})$ (erg s^{-1}) (6)	FWHM			$\log(M_{\text{BH}})$ (M_{\odot}) (10)	$\log L_{\text{bol}}$ (erg s^{-1}) (11)	λ_{Edd} (12)
						He I (km s^{-1}) (7)	Pa β (km s^{-1}) (8)	NIR (km s^{-1}) (9)			
2MASX J05054575–2351139	0.0350	2	–	5.80	44.24	1772^{+419}_{-318}	...	1772^{+419}_{-318}	7.37 ± 0.18	45.50	0.849
2MASX J18305065+0928414	0.0190	2	–	4.45	42.40	3513^{+232}_{-213}	...	3513^{+232}_{-213}	7.04 ± 0.09	43.09	0.009
ESO 234-G-050	0.0088	2	0.8	6.30	42.29	1110^{+63}_{-59}	1304^{+381}_{-322}	1128^{+106}_{-106}	6.00 ± 0.10	42.98	0.076
ESO 374-G-044	0.0284	2	–	6.96	43.57	1123^{+383}_{-221}	1412^{+318}_{-294}	1265^{+215}_{-215}	6.74 ± 0.15	44.71	0.742
MCG -01-24-12	0.0196	2	–	6.32	43.55	–	2069^{+300}_{-280}	2069^{+300}_{-280}	7.16 ± 0.12	44.24	0.096
MCG -05-23-16	0.0085	2	6.8	5.84	43.51	2474^{+67}_{-64}	2133^{+93}_{-89}	2278^{+162}_{-162}	7.22 ± 0.06	44.20	0.075
Mrk 1210	0.0135	2	–	6.92	43.35	1305^{+73}_{-32}	1936^{+118}_{-225}	1502^{+108}_{-108}	6.78 ± 0.06	44.36	0.303
NGC 1052	0.0050	2	1.5^a	5.12	42.22	2417^{+143}_{-128}	–	2417^{+143}_{-128}	6.63 ± 0.09	42.91	0.015
NGC 1365	0.0055	1.8	5.2	7.31	42.63	–	1971^{+85}_{-75}	1971^{+85}_{-75}	6.65 ± 0.09	43.32	0.037
NGC 2992	0.0077	2	5.1^a	6.25	42.55	3157^{+586}_{-400}	2055^{+29}_{-30}	2218^{+190}_{-190}	6.72 ± 0.08	43.24	0.026
NGC 4395	0.0013	1.9	4.0	6.32	40.79	1332^{+93}_{-70}	851^{+29}_{-34}	990^{+72}_{-72}	5.14 ± 0.07	41.48	0.017
NGC 6221	0.0050	2	3.2	7.41	42.05	2141^{+110}_{-141}	2256^{+99}_{-82}	2195^{+155}_{-155}	6.46 ± 0.06	42.74	0.015
NGC 7314	0.0048	1.9	4.4	5.70	42.42	1427^{+46}_{-38}	1347^{+46}_{-39}	1384^{+99}_{-99}	6.24 ± 0.06	43.11	0.058
NIR data taken from the literature											
IRAS F 05189-2524	0.0426	2	...	6.26	43.72	...	2619^b	2619	7.45 ± 0.10	44.41	0.073
Mrk 348 ^c	0.0150	2/FSRQ	...	5.51	43.90	1917^{+146}_{-131}	1514^{+416}_{-319}	1830^{+170}_{-170}	7.23 ± 0.08	44.98	0.448
NGC 1275 ^c	0.0176	2	...	6.91	43.71	2547^{+20}_{-24}	2824^{+98}_{-85}	2671^{+179}_{-179}	7.46 ± 0.06	44.40	0.069
NGC 7465	0.0065	2	...	5.78	42.14	...	2300^d	2300	6.54 ± 0.10	42.83	0.015

Notes. (1) AGN name; (2)–(3) redshift, source classification (from Baumgartner et al. 2013); (4) optical–NIR extinction; (5) mid-IR 4.6–22 μm colour; (6) 14–195 keV intrinsic luminosity (from Baumgartner et al. 2013); (7)–(8) intrinsic (corrected for instrumental resolution) FWHM of the broad emission-line component of the He I and Pa β from Onori et al. (2017); (9) Average FWHM of the He I and Pa β lines; (10) M_{BH} derived with the virial relation a3 of table 4 from Ricci et al. (2017). A constant virial factor $f = 4.31$ (Grier et al. 2013) has been adopted. An uncertainty $\epsilon \simeq 0.5$ dex, due to the spread of the population, should also be taken into account (Ricci et al. 2017). (11)–(12) bolometric luminosity and corresponding Eddington ratio, both calculated adopting the K -correction of Vasudevan & Fabian (2007).

^aFrom Burtscher et al. (2015);

^bMeasure of the FWHM of the Pa α line from Cai et al. (2010);

^cThe FWHM have been measured applying the fitting procedure described by Onori et al. (2017) on the data published by Riffel et al. (2006);

^dFrom Ramos Almeida, Pérez García & Acosta-Pulido (2009).

$M_{\text{vir}} = 6.3 \pm 0.7 \times 10^6 M_{\odot}$ (see table 1 in Ho & Kim 2014, and references therein). In Fig. 1 (top panel), we show the L_{14-195} distribution of all the AGN1 included in the *Swift*/BAT 70-month catalogue (blue dashed line) as well as the distribution of the control sample of 33 AGN1 (blue dotted line). The average X-ray luminosity is $\log L_{14-195} = 44.3$ with a spread $\sigma(\log L_{14-195}) = 1.0$ and $\log L_{14-195} = 43.8$ with a spread $\sigma(\log L_{14-195}) = 1.0$, for the *Swift*/BAT AGN1 and the control sample of AGN1, respectively.

3 COMPARISON BETWEEN THE AGN1 AND AGN2 POPULATIONS

As discussed by Landt et al. (2008), Onori et al. (2017) and Ricci et al. (2017), the most relevant NIR emission lines of the BLR (Pa α , Pa β , He I $\lambda 1.083 \mu\text{m}$) have, within the errors, the same FWHM. Therefore, a more robust BLR FWHM measure can be obtained using the average width (FWHM_{NIR}) of these lines (when available). In Fig. 1 (bottom panel), we show the FWHM_{NIR} of the BLR, derived using the He I and Pa β lines, as a function of the intrinsic X-ray luminosity L_{14-195} for both the AGN1 (blue open squares) and the AGN2/BLR (red filled circles) samples. Of the 33 AGN1, only the 20 with NIR emission-line measurements are plotted. As expected from the studies of the AGN X-ray LF (e.g. Ueda et al. 2003; La Franca et al. 2005; Ueda et al. 2014), AGN1 have, on average, larger luminosities than AGN2. However,

in the luminosity range where the two distributions overlap, $42.5 < \log L_{14-195} < 44.5$, AGN1 show significantly larger FWHM than AGN2: $\sim 3400 \text{ km s}^{-1}$ instead of $\sim 1970 \text{ km s}^{-1}$ ($\log(\text{FWHM}) = 3.531 \pm 0.036$ and $\log(\text{FWHM}) = 3.294 \pm 0.032$ for AGN1 and AGN2/BLR, respectively).

In order to compute the AGN2 M_{BH} , we have used the relation

$$\log \left(\frac{M_{\text{BH}}}{M_{\odot}} \right) = 7.75 + \log \left[\left(\frac{\text{FWHM}_{\text{NIR}}}{10^4 \text{ km s}^{-1}} \right)^2 \left(\frac{L_{14-195 \text{ keV}}}{10^{42} \text{ erg s}^{-1}} \right)^{0.5} \right], \quad (1)$$

which is based on the measure of the average FWHM observed in the NIR and the hard X-ray 14–195 keV luminosity. The relation has been calibrated by Ricci et al. (2017, see solution a3 in their table 4) assuming a common virial factor $f = 4.31$ (Grier et al. 2013, but see the discussion about this assumption in Section 4). According to the above equation, the measure of M_{BH} depends on the square root of the luminosity (as typical in the single epoch virial relations; Vestergaard 2002) and the square power of the FWHM. Therefore, the observed narrower (by a factor of ~ 0.25 dex) FWHM in the AGN2 sample implies (a factor of $0.5 = 2 \times 0.25$ dex) smaller M_{BH} for AGN2, if compared with AGN1 of the same luminosity.

In Fig. 2, the M_{BH} as a function of L_{14-195} of the AGN1 (blue open squares) and AGN2/BLR (red filled circles) samples is shown. For the AGN1 sample, M_{BH} has been derived using the RM technique.

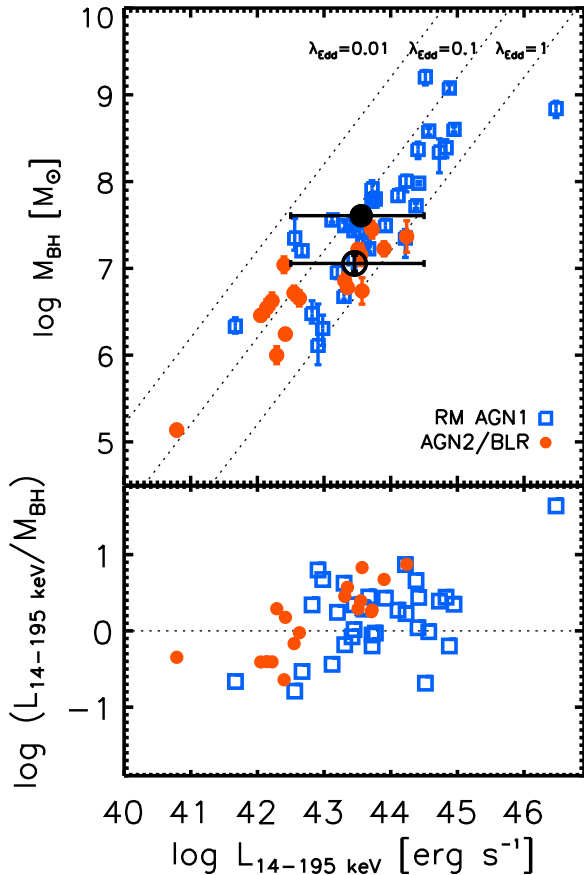


Figure 2. Top panel: BH masses of AGN1 (blue open squares) and AGN2/BLR (red filled circles) as a function of L_{14-195} . The black filled (open) circle shows the average M_{BH} value of the total AGN1 (AGN2/BLR) sample in the $42.5 < \log(L_{14-195} / \text{erg s}^{-1}) < 44.5$ luminosity bin and has been plotted at the position of the average $\log L_{14-195}$. The dotted lines show, as a reference, the location of constant λ_{Edd} , derived assuming a constant $L_{\text{bol}} = 20L_{14-195}$. Bottom panel: ratio between L_{14-195} and M_{BH} (plus a constant) of the AGN1 (blue open squares) and AGN2/BLR (red filled circles) as a function of L_{14-195} .

As also shown in Fig. 3, the M_{BH} of AGN2/BLR (red continuous line) is typically smaller than AGN1 (blue dotted line). The average (largest) M_{BH} is $\log(M_{\text{BH}}/M_{\odot}) \sim 6.8$ (~ 7.5) in the AGN2 sample, while in the control AGN1 sample, it is $\log(M_{\text{BH}}/M_{\odot}) \sim 7.6$ (~ 9.2). In the $42.5 < \log(L_{14-195} / \text{erg s}^{-1}) < 44.5$ luminosity bin, the average M_{BH} of the AGN2 sample is ~ 0.5 dex smaller than that measured in the AGN1 sample ($\log(M_{\text{BH}}/M_{\odot}) = 7.08 \pm 0.10$ and $\log(M_{\text{BH}}/M_{\odot}) = 7.61 \pm 0.01$, for AGN2/BLR and AGN1, respectively). For the sub-sample of 20 AGN1 for which the FWHM_{NIR} measurements are available, the average M_{BH} obtained using equation (1), instead of using the RM measurements, is very similar: $\log(M_{\text{BH}}/M_{\odot}) = 7.63 \pm 0.01$.¹

The above result is also illustrated in Fig. 2 (bottom panel), where the L_{14-195}/M_{BH} ratio (which is a proxy of the Eddington ratio λ_{Edd}), plus a constant, is shown as a function of L_{14-195} . We computed the Eddington ratio assuming the bolometric correction of Vasudevan

¹ Indeed, equation (1) has been calibrated by Ricci et al. (2017) using almost the same RM AGN1 of the control sample (31 out of 37 objects are in common).

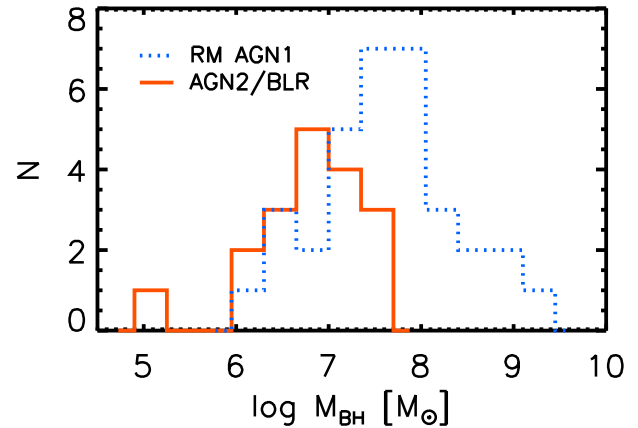


Figure 3. Distribution of M_{BH} of our sample of AGN2/BLR (red continuous line) and of the control sample of AGN1 whose M_{BH} have been measured via RM (blue dotted line). The M_{BH} have been computed assuming $f = 4.31$ for both samples (Grier et al. 2013, see the text for more details).

& Fabian (2007)² (see Table 1). In the overlapping luminosity bin $42.5 < \log(L_{14-195} / \text{erg s}^{-1}) < 44.5$, AGN2 have, on average, 0.3 dex larger λ_{Edd} than AGN1 ($\log \lambda_{\text{Edd}} \simeq -0.85$ and 1.15, for AGN2/BLR and AGN1, respectively).

4 ANALYSIS OF POSSIBLE SELECTION EFFECTS

Although based on few tens of objects, at face value, our results imply that AGN2 have, on average, about 0.25 dex lower BLR FWHM, and 0.5 dex lower M_{BH} (larger λ_{Edd}) than AGN1 of the same luminosity. In Onori et al. (2017), we have investigated whether our FWHM measurements could be affected by some selection biases. No dependence was found in the sample where the BLR was measured on both the X-ray and NIR fluxes, on the orientation angle of the host galaxy or on the hydrogen column density, N_{H} , measured in the X-ray band.

A possible selection could be originated by the effects of the absorption/reddening medium along the line of sight, which is obviously present as it is at the origin of the AGN2 classification, and then large N_{H} values ($> 10^{21} \text{ cm}^{-2} \text{ s}^{-1}$) are typically measured in AGN2. One scenario could be that the most central parts of the BLR are embedded in a region of absorbing material and the broad components that we have detected originate in the outer, and therefore slower, part of the BLR. In this case, a trend should be visible where the largest FWHM are detected in the less X-ray absorbed and/or less reddened objects. As shown in Fig. 4, where we plot the FWHM as a function of N_{H} and as a function of the extinction A_{V} , we do not find such trends in our AGN2 sample. The extinction A_{V} has been estimated in eight AGN2 using either the BLR Paschen and Balmer line ratios (when available), assuming a Milky Way reddening law (Allen 1976) and $R_{\text{V}} = 3.1$, or the values derived by Burtscher et al. (2015) using a ‘dust colour’ method (see Table 1). The measured $A_{\text{V}}-N_{\text{H}}$ distribution of our AGN2 sample is typical of the AGN2 population (see e.g. Burtscher et al. 2016, fig. 3).

² As parametrized by Shankar, Weinberg & Miralda-Escudé (2013, equation 22, in which, because of a typo, $\log L_{\text{X}}$ should read $\log \lambda_{\text{Edd}}$). No significant difference in the results was found by using the bolometric correction of Marconi et al. (2004).

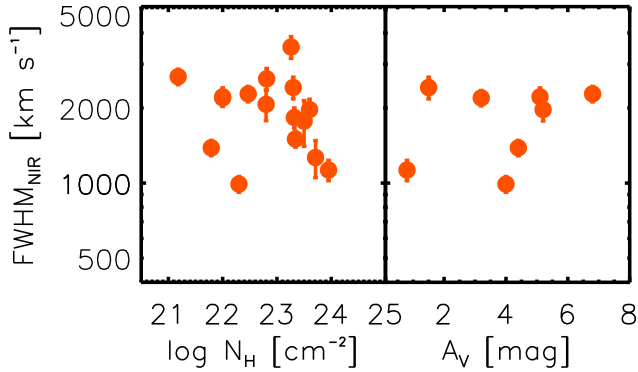


Figure 4. Left-hand panel: average FWHM of the BLR components of the NIR He I and Pa β lines of the AGN2/BLR as a function of the hydrogen column density N_{H} . Right-hand panel: same as the left-hand panel but as a function of the extinction A_{V} .

The presence of dust inside the BLR is unlikely as it would disagree with the results obtained through dust RM at K -band wavelength, so that the time lag of the inner radius of the torus is three to four times longer than the $H\beta$ time lag (Burtscher et al. 2013; Vazquez et al. 2015, and references therein). The dust, instead, is consistent with being originated at the distance of the predicted graphite sublimation radius (Netzer & Laor 1993; Netzer 2015). This implies that the BLR is indeed bound by the dust distribution, as also observationally confirmed by Landt et al. (2014, but see Czerny & Hryniewicz 2011 for a different scenario in which the BLR is originated in regions where dust could co-exist).

We can therefore conclude that, once a BLR component is detected, the dusty region (maybe clumpy, according to recent studies; Marinucci et al. 2016, and references therein) that surrounds the AGN should have been completely penetrated. Note that a possible consequence of dust absorption could be the reduction of the line intensity (but not of the BLR FWHM; see also Kim et al. 2015a). This could affect the estimation of the BH mass, if the line luminosity were to be used, as it is the case of some virial relations for type 1 AGN. Therefore, in the case of obscured AGN, instead than the optical/NIR line luminosities, it is better to use the hard X-ray luminosities as a proxy of the BLR radius in the virial relations for the estimation of the BH mass.

Another possible bias could be due to the fact that in the standard unification model, obscured AGN are viewed, on average, at larger angles relative to the accretion disc axis than unobscured AGN. Therefore, the estimation of the BLR FWHM could be affected by projection effects. Indeed, the dependence of BLR linewidths in terms of orientations is observationally well known (Wills & Browne 1986). Recently, Bisogni, Marconi & Risaliti (2017), using the EW of the [O III] $\lambda 5007$ Å line as an inclination indicator, have found that the more inclined AGN1 have, on average, larger FWHM of the BLR $H\beta$ line. These results match with those of Pancoast et al. (2014), who found that the virial f factor decreases with increasing inclination (see also Risaliti, Salvati & Marconi 2011). A smaller f factor is needed to compensate the increasing broadening of the FWHM with the inclination of the observed emission-line width. These results have been interpreted as a hint at a possible disc-like shape for the BLR (Bisogni et al. 2017).

However, the EW of the [O III] line is not a good indicator of the orientation for AGN2, as the AGN continuum component is suppressed and overwhelmed by the host galaxy contribution. Therefore, following Rose et al. (2015), we have used the $W2-W4$ (4.6–22 μm) mid-IR colour, as measured by the *Wide-Field In-*

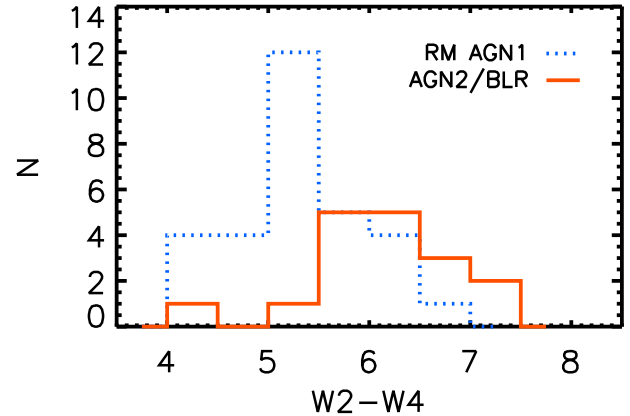


Figure 5. Distribution of the $W2-W4$ MIR colour of our sample of AGN2/BLR (red continuous line) and of the control sample of AGN1 whose M_{BH} have been measured via RM (blue dotted line).

frared Survey Explorer (Wright et al. 2010), to roughly estimate the orientation of our samples of AGN. In Table 1, the $W2-W4$ colours of the AGN2/BLR sample are listed. The more inclined AGN2 should show redder $W2-W4$ colours than AGN1, because the hottest dust emission of the inner regions of the torus should be less visible as the inclination increases (Rose et al. 2015, and references therein). Our AGN2/BLR show a red $W2-W4$ distribution, typical of the AGN2 population, having, an average, $\langle W2-W4 \rangle = 6.2$ with a (1σ) spread of 0.8, while the AGN1 control sample has $\langle W2-W4 \rangle = 5.2$ with a (1σ) spread of 0.7 (see Fig. 5 and, for comparison, fig. 2 in Rose et al. 2015). If the common luminosity bin $42.5 < \log L_{14-195} / \text{erg s}^{-1} < 44.5$ is considered, AGN2/BLR (AGN1) have $\langle W2-W4 \rangle = 6.4$ (5.4) with a (1σ) spread of 0.6 (0.7).

We can conclude that the smaller BLR FWHM and lower M_{BH} of our sample of AGN2 with respect to the AGN1 of the same luminosity should not be ascribed to orientation effects. Indeed, the larger inclination of the AGN2 should cause larger FWHM to be observed, and even smaller f factors to be used. Therefore, following Pancoast et al. (2014), even smaller M_{BH} could be derived for the AGN2/BLR sample than those obtained in this work, where a common $f = 4.31$ factor, for both AGN1 and AGN2, is assumed.

5 CONCLUSIONS

Determining the distribution of M_{BH} of AGN is of paramount importance in order to understand the AGN phenomenon.

Using deep NIR spectroscopic observations, we have detected faint BLR components in a sample of 17 AGN2 (Onori et al. 2017) drawn from the 14–195 keV X-ray *Swift*/BAT 70-month catalogue, which is free of biases against absorbed sources up to $\log N_{\text{H}} \lesssim 24 \text{ cm}^{-2}$ (Burlon et al. 2011). No dependence was found on the BLR detection success rate, or FWHM of the lines, on either the X-ray or NIR fluxes, or on orientation angle of the host galaxy, on the hydrogen column density and on the extinction.

In this work, we have found that the average AGN2 FWHM of the BLR is ~ 0.25 dex smaller than measured in a control sample of AGN1 having the same average X-ray intrinsic luminosity. Using new virial relations calibrated by Ricci et al. (2017), which are based on the FWHM of the most relevant BLR NIR emission lines and the intrinsic hard X-ray luminosity, we have measured the M_{BH} of the AGN2 in our sample. The M_{BH} of the AGN2 are, on average, ~ 0.8

dex smaller than measured in the control sample of AGN1. If AGN1 and AGN2 of the same luminosity $\log(L_{14-195}/\text{erg s}^{-1}) \sim 43.5$ are compared, AGN2 have 0.5 dex smaller BH masses than the AGN1.

Our findings are based on small samples and more observations are needed for more robust statistical grounds. However, at face value, our result disagrees with the standard AGN unification scenarios in which AGN1 and AGN2 are the same objects observed along different viewing angles with respect to a toroidal absorbing material.

Our findings could instead fit in an evolutionary scenario (see e.g. Hopkins et al. 2005) in which AGN2 represents the preceding stage of a type 1 AGN. In this picture, AGN2 are dust-enshrouded ‘buried’, low-mass ($M_{\text{BH}} \lesssim 10^{7.5} M_{\odot}$) BHs that accrete at high Eddington ratios. When feedback from the accretion drives away the obscuring material, a window is created in which the AGN is seen as an optical type 1. In this evolutionary path, highly accreting red quasars, as those observed by Kim et al. (2015b), could belong to an intermediate population. Eventually, the activity ends when the accretion rate drops below that required to maintain the typical AGN luminosities.

ACKNOWLEDGEMENTS

We thank the referee for her/his very useful comments that improved the manuscript. We also thank Robert Antonucci, Ryan Hickox and Cesare Perola for useful discussions. This paper is based on observations made with ESO telescopes at the Paranal Observatory and the Large Binocular Telescope (LBT) at Mt. Graham, Arizona. We acknowledge funding from PRIN-MIUR 2010 and from PRIN-INAF 2011. MB acknowledges support from the FP7 Career Integration Grant ‘eEASy’ (CIG 321913). RM acknowledges support from the ERC Advanced Grant 695671 ‘QUENCH’ and from the Science and Technology Facilities Council (STFC).

REFERENCES

- Allen C. W., 1976, *Allen: Astrophysical Quantities*, 3rd edn. Athlone Press, London
- Allevato V. et al., 2014, *ApJ*, 796, 4
- Antonucci R., 1993, *ARA&A*, 31, 473
- Baldassare V. F. et al., 2016, *ApJ*, 829, 57
- Baumgartner W. H., Tueller J., Markwardt C. B., Skinner G. K., Barthelmy S., Mushotzky R. F., Evans P. A., Gehrels N., 2013, *ApJS*, 207, 19
- Bisogni S., Marconi A., Risaliti G., 2017, *MNRAS*, 464, 385
- Blandford R. D., McKee C. F., 1982, *ApJ*, 255, 419
- Burlon D., Ajello M., Greiner J., Comastri A., Merloni A., Gehrels N., 2011, *ApJ*, 728, 58
- Burtscher L. et al., 2013, *A&A*, 558, A149
- Burtscher L. et al., 2015, *A&A*, 578, A47
- Burtscher L. et al., 2016, *A&A*, 586, A28
- Cai H.-B., Shu X.-W., Zheng Z.-Y., Wang J.-X., 2010, *Res. Astron. Astrophys.*, 10, 427
- Czerny B., Hryniewicz K., 2011, *A&A*, 525, L8
- Elitzur M., 2012, *ApJ*, 747, L33
- Graham A. W., 2008, *ApJ*, 680, 143
- Greene J. E., Ho L. C., 2007, *ApJ*, 667, 131
- Greene J. E. et al., 2010, *ApJ*, 723, 409
- Grier C. J. et al., 2013, *ApJ*, 773, 90
- Heckman T. M., Kauffmann G., Brinchmann J., Charlot S., Tremonti C., White S. D. M., 2004, *ApJ*, 613, 109
- Ho L. C., Kim M., 2014, *ApJ*, 789, 17
- Hopkins P. F., Hernquist L., Martini P., Cox T. J., Robertson B., Di Matteo T., Springel V., 2005, *ApJ*, 625, L71
- Kelly B. C., Vestergaard M., Fan X., Hopkins P., Hernquist L., Siemiginowska A., 2010, *ApJ*, 719, 1315
- Kim D., Im M., Kim M., 2010, *ApJ*, 724, 386
- Kim D. et al., 2015a, *ApJS*, 216, 17
- Kim D., Im M., Glikman E., Woo J.-H., Urrutia T., 2015b, *ApJ*, 812, 66
- Kormendy J., Bender R., Cornell M. E., 2011, *Nature*, 469, 374
- La Franca F. et al., 2005, *ApJ*, 635, 864
- La Franca F. et al., 2015, *MNRAS*, 449, 1526
- La Franca F., Onori F., Ricci F., Bianchi S., Marconi A., Sani E., Vignali C., 2016, *Frontiers Astron. Space Sci.*, 3
- Landt H., Bentz M. C., Ward M. J., Elvis M., Peterson B. M., Korista K. T., Karovska M., 2008, *ApJS*, 174, 282
- Landt H., Bentz M. C., Peterson B. M., Elvis M., Ward M. J., Korista K. T., Karovska M., 2011, *MNRAS*, 413, L106
- Landt H., Ward M. J., Elvis M., Karovska M., 2014, *MNRAS*, 439, 1051
- Lanzuisi G. et al., 2015, *A&A*, 573, A137
- Lusso E. et al., 2012, *MNRAS*, 425, 623
- Maiolino R., Shemmer O., Imanishi M., Netzer H., Oliva E., Lutz D., Sturm E., 2007, *A&A*, 468, 979
- Marconi A., Risaliti G., Gilli R., Hunt L. K., Maiolino R., Salvati M., 2004, *MNRAS*, 351, 169
- Marinucci A. et al., 2016, *MNRAS*, 456, L94
- Netzer H., 2015, *ARA&A*, 53, 365
- Netzer H., Laor A., 1993, *ApJ*, 404, L51
- Onori F. et al., 2017, *MNRAS*, 464, 1783
- Pancoast A., Brewer B. J., Treu T., Park D., Barth A. J., Bentz M. C., Woo J.-H., 2014, *MNRAS*, 445, 3073
- Peterson B. M., 1993, *PASP*, 105, 247
- Ramos Almeida C., Pérez García A. M., Acosta-Pulido J. A., 2009, *ApJ*, 694, 1379
- Ricci F., La Franca F., Onori F., Bianchi S., 2017, *A&A*, 598, A51
- Riffel R., Rodríguez-Ardila A., Pastoriza M. G., 2006, *A&A*, 457, 61
- Risaliti G., Salvati M., Marconi A., 2011, *MNRAS*, 411, 2223
- Rose M., Elvis M., Crenshaw M., Glidden A., 2015, *MNRAS*, 451, L11
- Schulze A. et al., 2015, *MNRAS*, 447, 2085
- Shankar F., Weinberg D. H., Miralda-Escudé J., 2013, *MNRAS*, 428, 421
- Ueda Y., Akiyama M., Ohta K., Miyaji T., 2003, *ApJ*, 598, 886
- Ueda Y., Akiyama M., Hasinger G., Miyaji T., Watson M. G., 2014, *ApJ*, 786, 104
- Vasudevan R. V., Fabian A. C., 2007, *MNRAS*, 381, 1235
- Vazquez B. et al., 2015, *ApJ*, 801, 127
- Veilleux S., Goodrich R. W., Hill G. J., 1997, *ApJ*, 477, 631
- Vestergaard M., 2002, *ApJ*, 571, 733
- Wills B. J., Browne I. W. A., 1986, *ApJ*, 302, 56
- Winter L. M., Lewis K. T., Koss M., Veilleux S., Keeney B., Mushotzky R. F., 2010, *ApJ*, 710, 503
- Wright E. L. et al., 2010, *AJ*, 140, 1868

This paper has been typeset from a $\text{\TeX}/\text{\LaTeX}$ file prepared by the author.